The mineralogy of arsenic in uranium mine tailings at the Rabbit Lake In-pit Facility, northern Saskatchewan, Canada

T. Pichler · M.J. Hendry · G.E.M. Hall

Abstract A detailed investigation of the mineralogy of As in the tailings of the Rabbit Lake uranium ore processing facility was conducted. The milling/ore extraction process was sampled at three different locations to obtain information about when, where and under what condition secondary As phases form. These samples were compared with four samples of varying As content from the Rabbit Lake in-pit tailings management facility (TMF). Up to 20% As in the tailings are present in primary minerals that reach the tailings directly because they are not dissolved during the uranium extraction. The remaining 80% constitute As that was dissolved during ore extraction and then re-precipitated before being discharged into the tailings pond. It was not possible to conclusively identify any individual re-precipitated (secondary) As minerals in the Rabbit Lake TMF. Indirect evidence from sequential extraction analyses suggests the presence of an amorphous Ca-As phase and a possible, but unlikely, minor amount of an amorphous Fe-As phase. However, the close association between hydrous ferric oxide (HFO) and As could be clearly demonstrated. HFO was identified to be 2-line ferrihydrite and its XRD pattern geometry indicates a substantial amount of adsorbed As. This is in good agreement with SEM, TEM and sequential extraction analyses that all showed the close association of HFO and As.

Keywords Arsenic · Hydrous ferric oxide · Mine tailings

Received: 14 February 2000 · Accepted: 9 May 2000

T. Pichler (✉)
Department of Geology, SCA528, University of South Florida, Tampa, FL 33620, USA
e-mail: pichler@chuma.cas.usf.edu
Tel: +1-813-9740321
Fax: +1-813-9742654

M.J. Hendry
Department of Geological Sciences, University of Saskatchewan, Saskatoon, Canada, S7N 5E2

G.E.M. Hall
Geological Survey of Canada, 601 Booth Street, Ottawa, Canada, K1A 0E8

Introduction

Tailings from a variety of mining operations can contain significant concentrations of arsenic (As), thus posing a potential environmental hazard. In particular, tailings from uranium and gold mines are known for their high As values. Increasing knowledge about the effects of long-term As exposure has caused the US EPA to lower the drinking water standards for As from 50 to 10 μg/l. Simultaneously, the requirements for de-regulation of mine waste deposits have become more stringent, putting pressure on the mining community to provide estimates about the long-term stability of As in mine tailings. Geochemical models (Langmuir and others 1999) that aim to predict the behavior of As following deposition of tailings, have to carefully identify the As phase(s) present. Only models that use the correct As phase(s) provide the necessary confidence on which to base decisions that may affect the environment for generations to come.

Ore processing ventures that are faced with high As contents in their mill feed, generally precipitate As as a stable phase that will withstand the physico-chemical conditions that exist in shallow groundwater regimes. Desired phases are calcium arsenates and scorodite ($FeAsO_4 \cdot 2H_2O$) whose precipitation is presumably initiated by adding lime and iron sulfate during the ore processing process (Rosehart and Lee 1972).

Mine tailings generally have a uniform particle size of < 125 μm and, therefore, are difficult to work with, because physical separation of individual minerals is as good as impossible. The relatively high detection limit of XRD analysis ($\sim 5\%$) negates the detection of minor constituents, such as secondary As minerals in bulk tailings material. Consequently, As minerals have not been conclusively described in mine tailings, often being referred to as scorodite-like minerals (Foster and others 1998).

The Rabbit Lake in-pit tailings management facility (TMF) is located in northern Saskatchewan, Canada (58°15′N; 103°40′E). Five separate uranium ore bodies (with different As concentrations) were processed at the

mill and tailings were deposited in layers in the TMF since startup in 1975. At present, the tailings body is ~425 m long, 300 m wide and 91 m thick at its center. The analysis of mill records indicates that the TMF contains over 17,000 tons of As. The physico-chemical conditions and the chemical distribution of As in the TMF have been investigated by Donahue and others (2000a,b). Based exclusively on sequential extraction analysis they concluded that 88% of the As is present as arsenates and the remaining 12% in the form of primary minerals. Being aware of the limitations of sequential extraction analysis, we decided to build on the work by Donahue and others (2000b), applying additional methods to evaluate the As mineralogy of the Rabbit Lake mine tailings.

Sample description and milling process

Samples 477, 481, 539 and 541 represent high (477 and 481) and low (539 and 543) As-containing tailings. They were collected in 1997 as drill core from the TMF. Details of the drilling and sampling procedures can be found elsewhere (Donahue and others 2000a).
Samples SOLPA (solution pachuca), CCD (countercurrent decantation circuit) and COM (combined) were collected in 1998 from the Rabbit Lake mill and represent different stages of the milling process. To understand why and where these samples were taken, it is necessary to summarize the milling process used at Rabbit Lake (Fig. 1). The ore is initially ground to a fine powder and then leached with H_2SO_4. During leaching most of the uranium and large fractions of associated elements (e.g. As, Mo, Ni and Fe) are dissolved. In the countercurrent decantation circuit (CCD, Fig. 1) the leach solution is separated from the remaining solids. From here the leach solution passes a sequence of extraction and precipitation events to separate the uranium. During this process, elements of no economic interest (e.g. As, Mo, Ni and Fe) are removed and treated in the solution pachuca. There, milk of lime ($Ca(OH)_2$) is added to achieve a final pH of ~10.5 and to initiate precipitation of saturated phases. The residue from the CCD circuit is also neutralized with milk of lime and then combined with the outflow from the solution pachuca to form the final tailings discharge. SOLPA is a sample of the solids from the last solution pachuca (of a series of three pachucas); CCD is a sample from the counter current decantation circuit; and COM represents the combined (actual) discharge from the mill to the TMF. Sample locations are also indicated in Fig. 1.

Analytical methods

A gravitational separation of samples COM, 477, 481, 539 and 541 was carried out in methyliodine water mixtures at four different densities (2.56, 2.63, 2.81 and 3.08 g/cm^3).

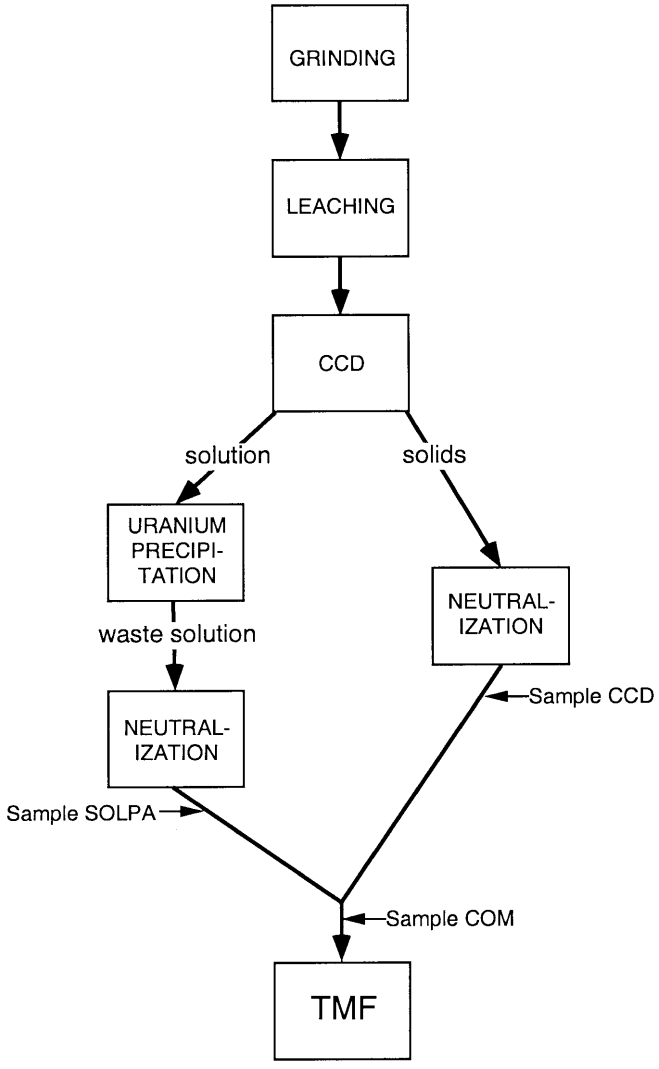

Fig. 1
Schematic diagram of the Rabbit Lake ore processing and uranium extraction operation. Sampling locations for SOLPA, CCD and COM are indicated. *CCD* indicates the countercurrent decantation circuit and *TMF* stands for tailings management facility

For transmission electron microscopy (TEM), air-dried samples were finely crushed with a glass mortar and dispersed in LR White embedding resin (Marivac, Halifax, Canada). Samples were twice infiltrated with the resin for 60 min before being re-suspended in fresh resin and polymerized at 60 °C for 1 h. Thin sections (80–90 nm) were cut with a diamond knife mounted onto an ultramicrotome (Reichert-Jung Ultracut E) and collected on carbon-coated Ni-grids having a supporting Formvar film. The thin sections were studied with a Philips EM400T electron microscope equipped with an X-ray spectrometer (LinK Analytical eXL/LZ-5) for elemental analysis. Energy dispersive spectroscopy (EDS) was performed at 100 kV with a beam current of 10 nA for ~100 s (live time). The diameter of the electron beam was 100 nm.

Table 1
Sequential extraction scheme for the Rabbit Lake tailings and mill samples

Series	Phase	Reagents	Procedure
A	Adsorbed/exchangeable elements	20 ml 1.0 M NaOAc (pH 8.2)	2-h leach, 2 × 5 ml H_2O rinse
B	Carbonates	20 ml 1.0 M NaOAc (pH 5.0)	2-h leach, 2 × 5 ml H_2O rinse
C	Hydrous iron oxides	20 ml 0.25 M NH_2OH HCl in 0.25 M HCl	2-h bath at 60 °C, 2 × 5 1ml H_2O rinse
D	Crystalline iron oxides	30 ml 1.0 M $NH_2OH \cdot HCl$ in 25% HOAc	3-h bath at 90 °C, 2 × 5 ml 25% HOAc rinse
E	Sulfides	8 ml Aqua Regia (6 ml HCl, 2 ml HNO_3)	Approximately 3-h bath (1 h at 90 °C)
F	Silicates and residuals	HCl–HF–$HClO_4$–HNO_3	Multi-acid digestion, residue redissolved in 3 ml HNO_3 and 1 ml HCl

Small sample chips and polished thin sections were examined with a stereo microscope. A selection of these were carbon-coated and mounted on aluminum stubs for SEM analysis on a Cambridge Stereoscan 360 scanning electron microscope, fully integrated with an Oxford Instruments (Link) eXL-II energy dispersive X-ray (EDX) microanalyzer.

The powder X-ray diffraction (pXRD) patterns were collected using an automated Philips X'Pert PW3710 system 2-22 powder diffractometer, stepping 0.02° 4θ from 2.00° to 82.00° 2θ, using copper X-radiation generated at 45 kV and 40 mA. Samples were mounted as acetone smears on a single-crystal silicon wafer low-background holder or as random powder mounts. XRD was carried out on bulk samples, gravitational separates and chemical separates.

Two subsamples of SOLPA (SOLPA-1 and SOLPA-2) were leached several times with water to dissolve the water-soluble fraction, thus facilitating the identification of insoluble minerals. Approximately 1 g (SOLPA-1) and 2 g (SOLPA-2) of SOLPA were leached three times with 50 ml of DDI for 30 min. The leach solutions were discarded after centrifuging and the samples were air-dried after the third leach.

SOLPA, CCD, COM and 481 were analyzed for the major elements, Ba, Sr, Y, Sc, Zr, and V by inductively coupled plasma emission spectrometry (ICP-ES); Cu, Zn, Ni, and Pb by inductively coupled plasma mass spectrometry (ICP-MS) and As by instrumental neutron activation analyses (INAA). FeO was determined by titration and S by infrared spectroscopy. Analyses were performed by Activation Labs in Ancaster, Ontario. Analytical errors (accuracy and precision) are estimated as follows: $<2\%$ for XRD, $<5\%$ for ICP-ES (except $<10\%$ Ba and Sr), $<10\%$ for ICP-MS and $\sim 10\%$ for INAA. Iron, As, Ni and Al in samples SOLPA-1 and SOLPA-2 were determined by ICP-MS at the University of Saskatchewan. Samples for ICP-MS and ICP-ES analyses were dissolved in HF-$HCLO_4$-HNO_3.

Sequential extraction analysis was carried out in six steps, (series A to F, Table 1) at the Geological Survey of Canada (GSC), using a procedure similar to that of Hall and others (1996), which was slightly modified to accommodate the slightly different mineralogy of the Rabbit Lake tailings. An overview is presented in Table 1. The samples 477, 481, 539, 543, and COM were not air-dried, thus representing in situ conditions in the TMF. Excess water was removed by centrifugation and the equivalent of 1 g of dry sample (ca. 1.5–2 g) was weighed into 50-ml polypropylene tubes for the sequential extraction. A second fraction of each sample of similar wet weight was taken, weighed and air-dried to report results with respect to the dry weight. Analytical quality was evaluated by including a control sample (Till-2, CCRICP) and a blank in every batch. Each sample was also run in duplicate.

Results

Sequential extraction

The results for the sequential extraction steps A to F are displayed in Fig. 2. The amounts of As, Fe, Ni, Al, Ca and Mg removed in each extraction step did not vary significantly between individual samples (Fig. 2). Slight variations were to be expected as a result of the different ore types that were processed at the Rabbit Lake facility (Donahue and others 2000a).

Approximately 20–25% As was removed during the leach, which extracts adsorbed/easily exchangeable elements and carbonates (Fig. 2a). The majority of As (up to 60%) was leached during the third step, which dissolves amorphous Fe-oxyhydroxides (HFO). Little As was removed during steps D and F that dissolve crystalline iron oxides and silicates respectively. Up to 18% was recovered while dissolving sulfides, step E. The majority of Fe was present either as an amorphous HFO or Fe-sulfide; very little to none was removed in steps A and B and $<12\%$ in steps D and F (Fig. 2b). Most of the Ni was removed during steps B, C and E that represent the carbonate, amorphous HFO and sulfide phases respectively (Fig. 2c). Most of the Al was removed during steps E and F ($>95\%$), with most residual Al leached during step C (Fig. 2d). More than 80% of the Ca was extracted in the first leach and remov-

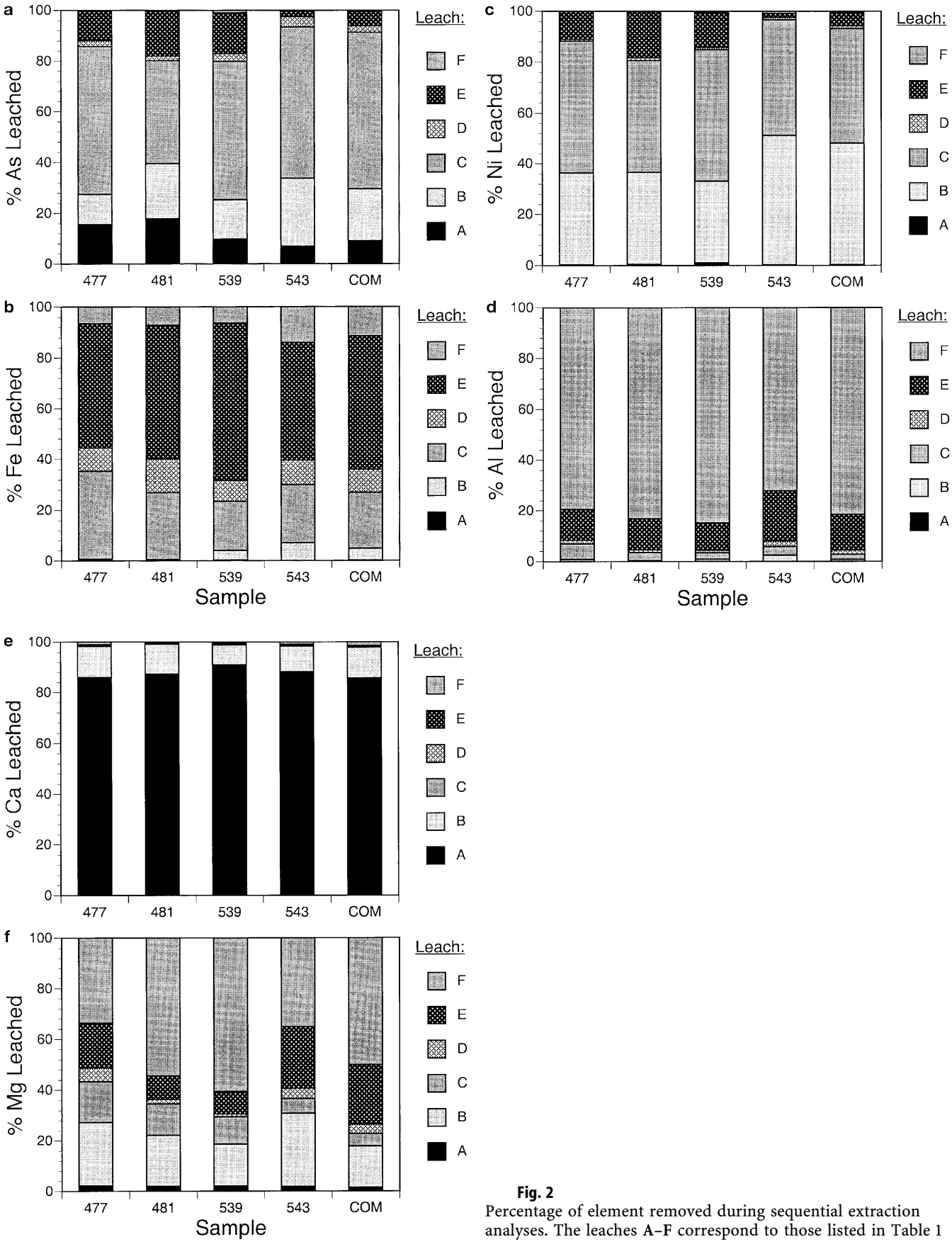

Fig. 2
Percentage of element removed during sequential extraction analyses. The leaches **A–F** correspond to those listed in Table 1

al was almost complete after the second (Fig. 2e). Most of the Mg was removed in the silicate leach, followed by the carbonate and the sulfide leaches. In samples 477, 481 and 539 a significant portion of Mg was also removed in leach B (amorphous HFO; Fig. 2f).

Powder X-ray diffraction

X-ray diffraction analyses were of limited use to determine the As location and/or mineral phase. Quartz, illite, chlorite, kaolinite and gypsum were the only minerals identified in the scans of bulk samples. Considering the concentration of As in the tailings, the nominal concentration of a possible As-bearing mineral should be $<5\%$, thus making its identification by XRD very difficult. There is no difference between the scans of COM (Fig. 3) and those of samples 477, 481, 539 and 547 independent of their As concentration. To increase the relative abundance of a possible As-bearing mineral the bulk samples were separated by gravitation. The X-ray scans of those separates showed: (1) an increase in clay minerals with decreasing specific weight of the separate; and (2) the presence of hematite and Fe, Ni and As sulfides in the heavy fraction (>3.08 g/cm^3). The peaks for As sulfides were stronger in sample 481 and the peaks for hematite were stronger in sample 539. The residue of each leach step (A–F) of the sequential extraction experiment was also scanned. As anticipated, this did not aid in the identification of As-minerals, because quartz, which is the dominant mineral in the tailings and therefore, in the XRD scans, was removed only in the last step of the sequential extraction.

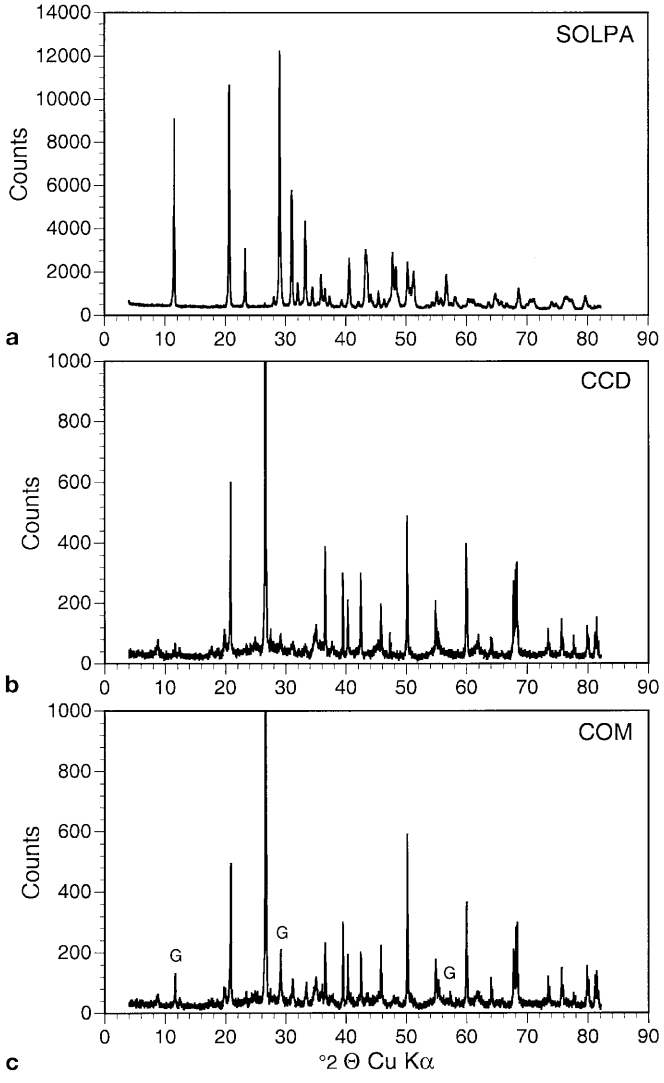

Fig. 3
X-ray diffractometer patterns for samples **a** SOLPA, **b** CCD and **c** COM. All peaks in the pattern of **a** SOLPA are accounted for by gypsum. The two patterns for CCD and COM clearly demonstrate the abundance of quartz and the presence and absence of gypsum in COM and CCD respectively

A direct comparison of the three samples that were collected directly in the Rabbit Lake mill confirms that COM is a mineralogical combination of CCD and SOLPA (Fig. 3). According to its XRD pattern, SOLPA is dominated by gypsum; no other minerals were identified during analysis of this pattern (Fig. 3a), although several peaks were higher than expected when compared with literature data. The sample CCD contains mainly quartz with minor amounts of clays and the sample COM contains quartz, gypsum and clays.

To further investigate the mineralogy of the sample SOLPA, we scanned the leach residues SOLPA-1 and SOLPA-2. Once gypsum was dissolved (SOLPA-1), the peaks for calcite became apparent (Fig. 4a) and with further removal of calcite, the scan in Fig. 4b revealed the presence of 2-line ferrihydrite (Chukhrov and others 1973).

Chemical composition

The chemical compositions of samples SOLPA, CCD, COM and 481 are listed in Table 2. SOLPA consists mainly of CaO and SO_4 and has high As and Ni concentrations. CCD consists mainly of SiO_2 and Al_2O_3 and has relatively low concentrations of As and Ni. COM is similar in composition to CCD, but has higher concentrations of As, Ni, CaO and SO_4. COM is the final tailings discharge, and thus a mixture of SOLPA and CCD, and therefore is intermediate in chemical composition between the two. Based on simple mass balance calculations using the element concentrations in SOLPA, CCD and COM, the fractions of SOLPA and CCD were determined to be $\sim$10–20% and 80–90% respectively (Table 3). The mass balance equation applied is:

$$x^*n(\text{SOLPA}) + y^*n(\text{CCD}) = n(\text{COM}),$$

where x and y are the fractions and n is the concentration of an element in its respective sample. The equation did not work for MgO, because slaked MgO is used in the uranium precipitation circuit for pH control (Brett Moldovan, CAMECO, personal communication). The use of $Fe_2O_3^T$ (where T = total concentration regardless of oxidation state) produced a significantly different mixture of SOLPA and CCD of 40 and 60% respectively. This can be

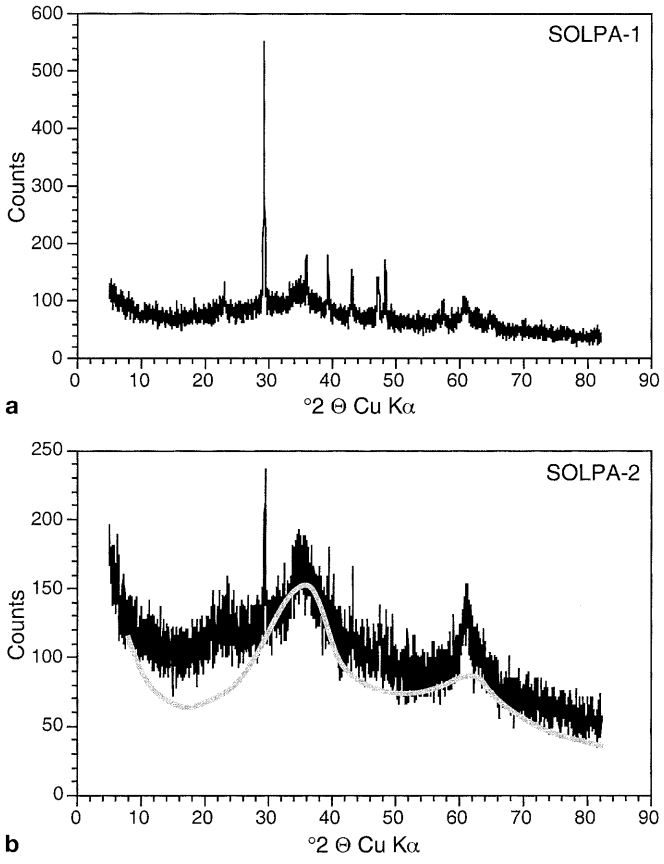

Fig. 4
X-ray diffractometer patterns for samples **a** SOLPA-1 and **b** SOLPA-2. These two scans represent the residue of SOLPA after extensive leaching with water. The removal of gypsum has allowed for the identification of calcite in SOLPA-1 and 2-line ferrihydrite in SOLPA-2. The solid, light gray line in the pattern of SOLPA-2 represents the XRD pattern of a naturally occurring As-rich 2-line ferrihydrite from Papua New Guinea (Pichler and others 1999)

attributed to two factors: (1) addition of iron from the physical degradation of the steel grinding balls, and (2) to a lesser extent from the addition of ferric sulfate in the impurity precipitation circuit (Brett Moldovan, CAMECO, personal. communication). The calculated ratios of SOLPA and CCD Sample 481 is similar in composition to COM, but has higher As and Ni concentrations.
The concentrations of Fe, As, Ni and Al for SOLPA-1 and SOLPA-2 are compared with those in SOLPA in Fig. 5. With the exception of As in SOLPA-2, all other elements showed a steady increase in concentration with increased leaching. This indicates the loss of elements other than those determined; in particular Ca, SO_4 and CO_3, as indicated by the absence of gypsum and the decline of calcite concentration in the XRD scans of SOLPA-1 and SOLPA-2 (Fig. 5).

Scanning electron microscopy (SEM)

The analysis of sample SOLPA revealed the presence of gypsum, which occurred as elongated crystals, and a fuz-

Table 2
Chemical composition of Rabbit Lake mill and tailings samples. *T* Total concentration regardless of oxidation state

Sample	SOLPA	CCD	COM	481
SiO_2 (%)	2.1	70.9	63.97	63.61
Al_2O_3 (%)	2.05	13.58	12.49	6.95
$Fe_2O_3^T$ (%)	3.47	0.74	1.84	0.33
FeO (%)	< 0.1	1.3	0.51	1.72
MnO (%)	0.1	0.01	0.03	0.03
MgO (%)	1.62	1.58	1.73	0.46
CaO (%)	26.3	1.3	4.44	6.26
Na_2O (%)	0.36	0.26	0.29	0.09
K_2O (%)	0.11	2.95	2.72	1.63
TiO_2 (%)	0.01	0.41	0.37	0.32
P_2O_5 (%)	0.25	0.06	0.07	0.02
LOI (%)	23.75	7.15	11.97	14.36
S^T (%)	13.1	0.91	2.13	3.05
SO_4 (%)	33.3	2.45	6.1	8.75
Total	93.43	101.39	106	102.8
As (ppm)	15000	623	3320	9610
Ba (ppm)	9	153	144	108
Cu (ppm)	285	49	84	327
Ni (ppm)	7096	221	1703	6696
Pb (ppm)	147	979	859	571
Sc (ppm)	33	7	11	7
Sr (ppm)	81	187	181	146
V (ppm)	355	222	255	277
Y (ppm)	265	18	53	44
Zn (ppm)	337	57	126	87
Zr (ppm)	9	206	188	383

Table 3
Calculated fractions of SOLPA and CCD present in the Rabbit Lake tailings discharge (COM). *nd* Not determined

Sample	SOLPA	CCD
SiO_2	0.10	0.90
Al_2O_3	0.09	0.91
$Fe_2O_3^T$	0.40	0.60
MnO	0.22	0.78
MgO	nd	nd
CaO	0.13	0.87
Na_2O	0.30	0.70
K2O	0.08	0.92
TiO_2	0.10	0.90
S^T	0.10	0.90
SO_4	0.12	0.88
As	0.19	0.81
Ba	0.06	0.94
Cu	0.15	0.85
Ni	0.22	0.78
Pb	0.14	0.86
Sc	0.15	0.85
Sr	0.06	0.94
V	0.25	0.75
Y	0.14	0.86
Zn	0.25	0.75
Zr	0.09	0.91

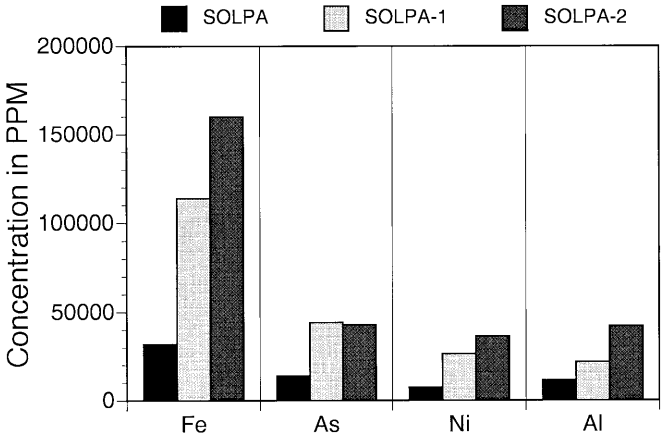

Fig. 5
Concentrations of Fe, As, Ni and Al in SOLPA, SOLPA-1 and SOLPA-2

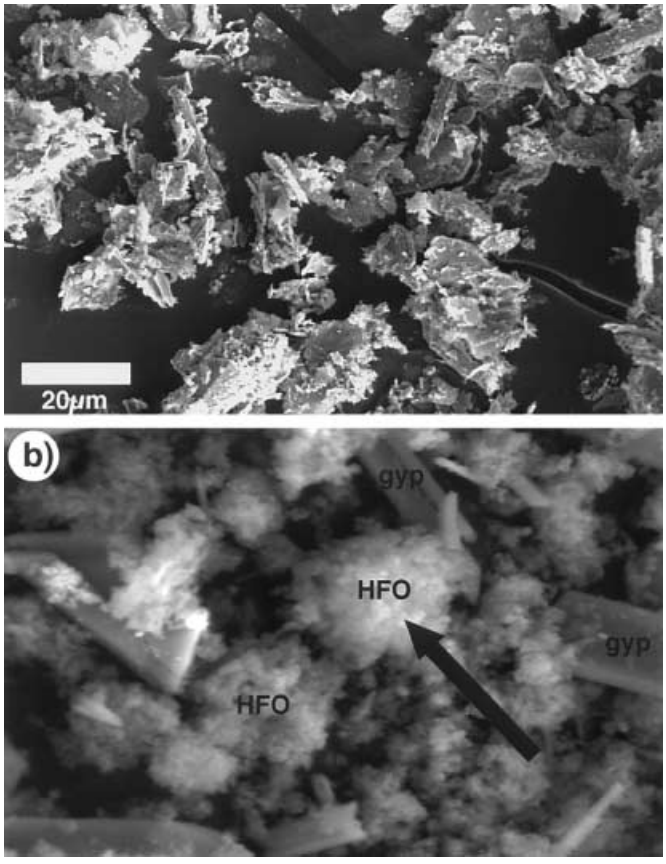

Fig. 6
SEM photo micrographs of samples **a** SOLPA and **b** 481. The needle-like shaped bodies in **a** are gypsum crystals (gyp) and the fuzzy, globular material is a possible mixture of ferrihydrite, Ni–Al hydroxide and Ca-arsenate. The arrow indicates a point from where an EDX spectrum was obtained. For more information see text. The arrow in the photomicrograph of sample 481 **b** indicates the occurrences of a fuzzy, globular material identical to that seen in **a**. The EDX spectra obtained from that point returned the same elemental composition as the one taken in **a**

zy appearing aggregate of ~20 to 30 μm in diameter (Fig. 6a). EDS analysis of the area marked in Fig. 6a revealed the following elements, listed in decreasing intensity: Ca, Al, Fe, S, Si, Mg, Ni, As, K and Cu. Figure 6b demonstrates the fine-grained character of the tailings material showing that most individual grains are <100 μm in size. A material similar in appearance and chemical composition to that shown in Fig. 6a was also found in all other samples. The EDS analysis of the area marked in Fig. 6b revealed the following elements, listed in decreasing intensity: Si, Ca, Ni, Fe, S, Al, Mg, As and Cu.
The analyses of polished thin sections made from samples 481 and 543 (a high and a low As sample) showed that only a few of the heavy minerals (bright appearance in back-scatter mode) in 543 contained As, whereas most heavy minerals in 481 were Ni-As sulfides. It was not possible to find the fuzzy appearing aggregates mentioned above during the analyses of the thin sections. This indicated that they are most likely too fragile or water soluble to survive the preparation process.
SEM analyses of individual grains that were separated from the bulk samples by a combination of gravitational separation and handpicking under a stereo microscope confirmed the observations that were made on bulk samples and on polished thin sections.

Transmission electron microscopy (TEM)

To overcome the problems that were caused by the three-dimensional character of the SEM analyses, samples SOLPA, COM and 481 were analyzed by TEM. This confirmed the presence of gypsum, hydrous ferric oxide (HFO) and a material primarily composed of Fe, As, Ni, Al, Ca and some S. The phases that were observed had a fuzzy, globular appearance (Fig. 7), characteristic of HFOs (Fortin and others 1993) and grain sizes were generally in the 0.5 to 2 μm range.
Representative chemical and structural compositions, obtained by EDS analyses, are presented in Table 4. Gypsum shows an appreciable Ca excess with a molar Ca/S ratio of 1.4 instead of 1. Other analyses fell into four distinct groups: As-Fe-rich, Al-Ni-As-Fe-rich, Ni-As-Fe-rich and Fe-rich (Table 4, analyses b–e). Nickel and Al are either approximately equal in concentration or Al is absent when Ni concentrations are high. Analysis d in Table 4 shows a very high As concentration compared with Fe. Analysis f represents the mineral illite. The illite composition is in good agreement with that published for illite (Deer and others 1992) and, therefore, suggests a relatively good reliability for the other analyses. Despite the substantial amount of EDS analyses that were performed, it was not possible to deduce a more systematic relationship between individual elements. This was partly because of the sampling uncertainty that arises because the diameter of the electron beam is ~100 nm, whereas the size of individual particles is less than that. Analyses, although performed side-by-side in an apparently homogenous area, did not produce the same chemical compositions.

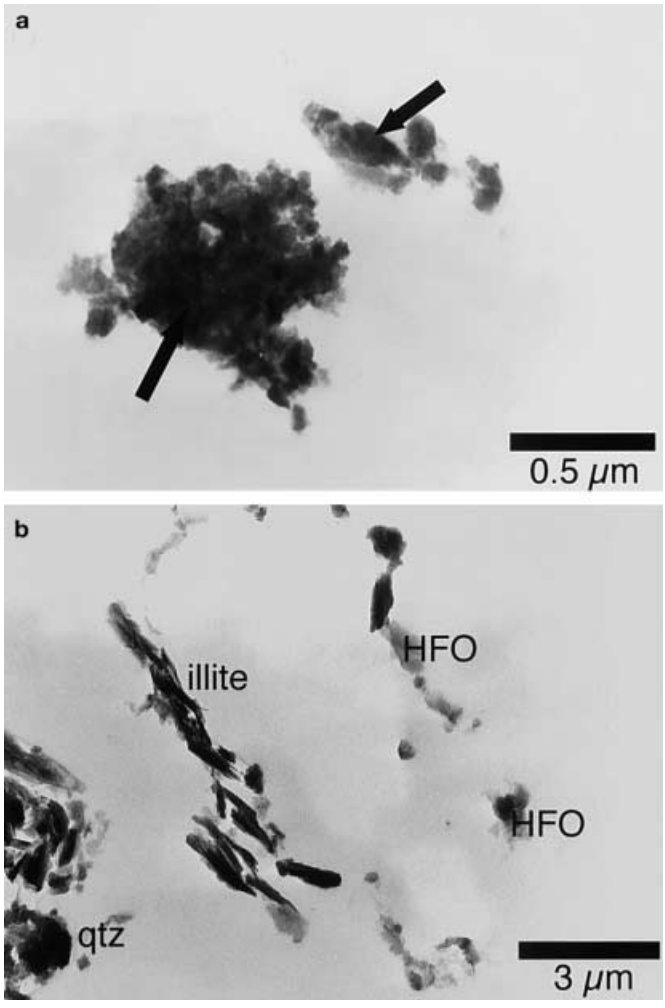

Fig. 7
TEM Photomicrographs of samples **a** SOLPA and **b** 481. Arrows indicate where semi-quantitative EDS measurements were performed

Discussion

The results of the analytical program identified three secondary minerals that were precipitated during the milling process at the Rabbit Lake facility: hydrous ferric oxide (HFO), gypsum and calcite. None of the minerals that were identified as secondary minerals is an As mineral; nevertheless, these minerals may incorporate As as impurities or adsorb As onto their surface. There is some indirect evidence that points towards the presence of Ni-Al hydroxides and Ca-arsenates and maybe Fe-arsenates. The only true As minerals we conclusively identified in the tailings were constituents of the uranium ore that were not dissolved in the extraction process and thus reached the TMF via the CCD fraction. These As minerals were detected mostly during the XRD analyses of the heavy fractions and during SEM analysis of handpicked particles. Minerals identified were rammelsbergite, nickeline, gerstorffite, arsenopyrite and bravoite. These findings are in agreement with those by researchers working on the mineralogy of the Rabbit Lake ore bodies (Donahue and others 2000a).

Hydrous ferric oxide (HFO)

The mobility and immobilization of As in natural waters is, in most circumstances, controlled by sorption onto particulate phases (Mok and Wai 1994). In particular, the HFO, 2-line ferrihydrite is known to have a great sorption affinity for both arsenite (As(III)) and arsenate (As(V)) and As/HFO associations are documented to occur in a variety of natural environments (Boyle and Jonasson 1973; Belzile and Tessier 1990; O'Neill 1990; Parker and Nicholson 1990). Because of the importance of this As/HFO association in both natural and anthropogenic settings (e.g. mine tailings) there have been several detailed mineralogical studies of synthetic As/HFO sorbate/sorbant materials and coprecipitates (Arneth and others 1989; Bowell 1994; Webster and Webster 1994; Manning and Goldberg 1997; Langmuir and others 1999). These studies have demonstrated the large sorption capacity of HFO for As, showing that sorption densities as high as 0.7 and 0.25 mole-As/mole-Fe can be obtained in coprecipitation and sorption experiments respectively (Fuller and others 1993). Several experimental studies have found that As(III) and As(V) adsorption at standard conditions (25 °C, 1 bar) is generally rapid and strongest at a pH of approximately 6–7 (Bowell 1994).

On first examination, the HFO sample (SOLPA-2) (Fig. 4b) shows two Bragg bumps at d-spacings of ~1.5 and 2.5 Å that are generally taken to be characteristic of 2-line ferrihydrite. This may lead to the conclusion that the samples are simply 2-line ferrihydrite and that no further information can be derived from the XRD patterns. XRD patterns, however, are directly related to the underlying radial distribution functions (i.e. angle-averaged Patterson functions that include all disorder and finite particle size effects), meaning that the differences in XRD pattern shapes translate into differences in populations of cation-cation, cation-anion, and to a lesser extent anion-anion distances. Aided by extended X-ray absorption fine structure (EXAFS) analysis, this concept was used by Waychunas and others (1996) to study synthetic As/HFO materials. In light of the latter study and the study of Pichler and others (1999), the higher intensity on the high d-spacing side of the As/HFO peaks of sample SOLPA-2 (when compared with As-free 2-line ferrihydrite, Jambor and Dutrizac 1998), can be interpreted as being directly caused by a significant population of Fe-As structural pairs, across shared bridging coordination oxygen anions on the surface. A similar As-O pair affects the 1.5-Å peak in As/HFOs and the general smearing out (broadening), relative to the Bragg peaks of 2-line ferrihydrite, is understood in terms of smaller X-ray coherent domains (i.e. smaller primary particles) in the As/HFO materials.

Scavenging of elements into and onto metal hydroxides is a result of coprecipitation, adsorption, surface complex formation, ion exchange, and penetration of the crystal

Table 4
Representative semi-quantitative EDS analyses for secondary phases in Rabbit Lake mill and tailings samples. *nd* Not determined; *HFO* hydrous ferric oxide; *AlNiH* aluminum nickel hydroxide; *FO* ferric oxide

Sample	SOLPA	SOLPA	SOLPA	481	481	481
Analysis	a	b	c	d	e	f
Phase[a]	Gypsum	HFO	HFO/AlNiH	HFO/NiH	HFO or FO	Illite
In wt%						
S	36.2	0.3	0.5	0.9	0.2	0.1
Si	0.2	6.2	14.1	10.3	4.4	49.7
Ca	62.9	2.2	2.1	1.5	0.4	0.1
Fe	0.5	57.6	38.3	28.4	89.7	2.4
As	<0.1	26.1	13.4	26.6	2.6	0.1
Al	nd	0.1	9.8	0.0	2.0	32.8
Ni	nd	6.0	21.1	33.8	0.2	0.1
P	nd	2.0	0.9	nd	nd	nd
K	nd	nd	nd	0.6	0.6	14.8
In atom%						
S	41.5	0.6	0.7	1.6	0.3	0.1
Si	0.3	12.1	23.0	20.3	8.6	51.8
Ca	57.8	3.0	2.5	2.1	0.5	0.1
Fe	0.3	56.6	31.5	28.1	83.8	1.2
As	<0.1	19.1	8.2	19.7	1.8	0.1
Al	nd	0.2	16.6	0.1	4.2	35.7
Ni	nd	5.6	16.4	31.9	0.1	0.1
P	nd	3.5	1.3	nd	nd	nd
K	nd	nd	nd	0.8	0.7	11.1
Atom ratios						
Ca/As	nd	0.16	0.30	0.11	0.28	1.00
Ni/Al	nd	28.0	0.99	319	0.02	0.001
Fe/As	nd	2.96	3.84	1.43	46.6	24.0

[a] Assumed phase that is purely based on the observed chemical composition

lattice (Chao and Theobald 1976). In natural systems, it is often impossible to distinguish between coprecipitation and adsorption (Drever 1988). Adsorption, however, has been observed to be the basis of most surface-chemical reactions (Stumm and Morgan 1996) making it the most likely cause for the As content in Rabbit Lake HFO. The relatively high As values (Table 4) are presumably achieved by a combination of the intrinsic nanocrystalline nature of 2-line ferrihydrite (typically 1–2 nm diameters) and the presence of As in solution at the time of HFO precipitation. Fuller and others (1993) noted that uptake was greater when As was present in solution during precipitation of HFO. Sorption sites on the newly formed HFO can be immediately occupied by As before they are destroyed by the continued precipitation of more HFO. It is this intrinsic relationship that makes adsorption and coprecipitation virtually indiscernible in natural systems.

TEM and SEM micrographs for samples SOLPA, COM and 481 are shown in Figs. 6 and 7. The agglomerations are composed of nanometer-scale HFO particles that are detected as dense spots in Fig. 7 and are typical of ferrihydrite particles seen at this magnification (Fortin and others 1993). These micrographs, combined with extensive TEM-based EDS measurements, allow us to conclude: (1) that there is no evidence for separate phases on this scale or phases other than the As-rich HFO outlined by XRD; (2) that the As/HFO particles are smaller than 100 nm (TEM beam size); and (3) that As/HFO particles are often associated with significant amounts of Ni and Al that presumably represent a Ni-Al hydroxide.

The close association between HFO and As is also demonstrated by the sequential extraction data. The largest amount of As was recovered during leach C (Fig. 2a), which is the step that was designed to dissolve amorphous oxy-hydroxide phases (Table 1).

The conclusion is that HFO must contain a significant amount of adsorbed (or coprecipitated) As. The XRD measurement (Fig. 4b) is significantly different from As-free 2-line ferrihydrite and similar to those of synthetic and natural As-rich HFO (Waychunas and others 1996; Pichler and others 1999). The As, however, is certainly not in a separate crystalline phase and there is evidence for Fe-As pairs that precludes most of the As from being in separate amorphous or nanocrystalline phases.

The large demonstrated As sorption densities suggest that the Rabbit Lake As-rich HFOs are intermediate between classic sorbate/sorbant systems and solid solutions or compounds in which the As and Fe occupy cation sites in a crystal structure that is more stable than a two-phase mixture. Indeed, the As is found to stabilize the HFO with respect to transformations to other oxides and

to complex to the HFO surface in such a way as to modify the local coordination environments of a significant fraction of the Fe (Waychunas and others 1996).

Arsenates

The precipitation of metal arsenates as an arsenic removal mechanism is a preferred method to treat mine-processing effluents (Rosehart and Lee 1972). At the TMF, the formation of calcium arsenates would be the most probable, because scaled lime ($Ca(OH)_2$) is added to the processing effluent as a pH control. The precipitation of arsenite phases is possible, but they are more soluble than their arsenate analogs (Robins 1985). Conditions in the Rabbit Lake TMF are oxidizing and As is dominated by arsenate (As^{5+}; Donahue and others 2000a,b), thus precipitation could proceed according to (Laguitton 1976):

$$4Ca^{2+} + 2AsO_4^{3-} + 2OH^- + 4H_2O = Ca_3(AsO_4)*Ca(OH)_2*4H_2O.$$

Despite the apparently ideal conditions of formation (abundant Ca^{2+}, high pH and As^{5+}) a discrete calcium arsenate phase was not detected in the course of the SEM, TEM and XRD investigations. This, however, does not preclude their existence, because modal abundance in the bulk material may have been too low to allow for detection by XRD. Their absence in the scans of SOLPA-1 and SOLPA-2 (Fig. 4) and during TEM analysis could be a result of sample treatment; calcium arsenates could have dissolved while the sample material was in contact with water.

A close association between Ca and the water-soluble As in the Rabbit Lake tailings is indicated by the results of our sequential extraction analyses and water leaches of sample SOLPA (Figs. 2 and 5). The passive accumulation of Fe, As, Ni, and Al in SOLPA-1 and SOLPA-2 is a result of the removal of other elements, in particular, Ca, SO_4 and CO_3 as indicated by the XRD scans in Fig. 4. In sample SOLPA-2, however, the As concentration did not increase, which implies its association with Ca. The molar Ca/SO_4 ratio in sample SOLPA is ~ 0.5 (Table 2), indicating that only half of the Ca is present as gypsum. Some of the remaining Ca is present in the form of calcite, but its modal abundance is clearly less than that of gypsum, as evidenced in our XRD patterns (Fig. 5). This leaves a substantial amount Ca unaccounted for. The possibility of As as an impurity in gypsum is highly unlikely given its low concentration in gypsum crystals that were analyzed by EDS (Table 4, analysis a). The close association between Ca and As is also evident from our sequential extraction data. A significant amount of As and almost all Ca were removed during our first two leaching steps (Figs. 2a,e). This is in agreement with findings of Donahue and others (2000b) who observed a similar trend in the As and Ca concentrations during sequential leaching of Rabbit Lake tailings.

The presence of Ca-arsenates is indicated by several lines of indirect evidence; however it was not possible to prove its presence as a crystalline Ca-As phase. Small amounts of a crystalline Ca-arsenate although unlikely, cannot be completely ruled out, because of the high detection limit of XRD. However, the extensive SEM and TEM analyses did not indicate any crystalline Ca-As phase. If Ca-arsenates are present as amorphous phases, their solubility is much higher than those for crystalline phases. Unfortunately, thermodynamic data are not available to evaluate the solubility of amorphous Ca-arsenates. Nevertheless, the leaching experiment of SOLPA (with water only) and steps A and B of the sequential extraction analyses clearly demonstrated the mobility of Ca and As. Geochemical models that address the long-term stability of As in mine tailings, therefore, have to carefully establish the As-phase(s) before choosing thermodynamic data to evaluate solubilities.

The precipitation of crystalline Ca-arsenates may be more likely if the pH at Rabbit Lake facility would be increased to 11.5 instead of its current value of 10.5. Above a pH of 11.5 arsenate ions (AsO_4^{3-}) dominate, thus enhancing the precipitation of Ca-arsenates if sufficient Ca^{2+} is available (Kelleher 1994).

The Fe-arsenate, scorodite ($FeAsO_4 \cdot 2H_2O$), is a desirable precipitate in mine tailings because of its relative low solubility (Rosehart and Lee 1972). Langmuir and others (1999) reported the precipitation of scorodite in processed uranium tailings from the JEB TMF in northern Saskatchewan. Unfortunately, however, they did not provide clear evidence for their measure of scorodite. Foster and others (1998), who investigated several California mine wastes, speculate that As^{5+} could be present in a precipitate such as scorodite, but did not detect it by either microprobe or XRD analyses. These findings suggest that scorodite is poorly crystalline or has low abundance.

The presence of scorodite, although highly unlikely in the tailings, cannot be completely ruled out. We did not find evidence for the presence of a crystalline Fe-As phase, but similar to the inferred presence of Ca-arsenate, there is some indication for the presence of an Fe-arsenate in the Rabbit Lake tailings samples 539, 543 and COM, where a minor amount of Fe was removed during our first two leaching steps (Fig. 2b). If present as amorphous phases, however, their solubility is much higher than those for crystalline analogs and the use of available thermodynamic data for crystalline scorodite may not be applicable to predict the long-term stability of As in mine tailings.

Al-hydroxide

Similar to its adsorption onto HFO, As can also sorb onto Al-phases, in particular gibbsite and alumina (Korte and Fernando 1991; Foster and others 1998). The Al concentrations in the tailings are high (Table 2), but most Al is present in primary clay minerals, as indicated by its behavior during sequential extraction (Fig. 2d). Thus, the availability of Al for the formation of a secondary Al-phase is minimal. Sample SOLPA contains 2.05 wt% Al_2O_3 (Table 2), corresponding to ~ 0.2 wt% in sample COM that would be available for the formation of secondary Al-phases. These low concentrations clearly put

secondary Al-phases out of reach for detection by XRD methods. Given the low abundance, adsorption of As onto Al-phases should be minimal, in particular when considering that As has to compete with Ni for sorption sites, because of the documented affinity between Ni and Al (Taylor 1974). Scheidegger and others (1998), for example, demonstrated the formation of a mixed Ni-Al phase, nucleating at the mineral-liquid interface of clay and oxide minerals.

The intricate interplay between Ni-Al hydroxides, HFO and As (Figs. 5 and 6; Table 4) is puzzling and its resolve is beyond this study. The close spatial relationship between these phases, however, indicates that they communally provide an environment that is beneficial for their formation (i.e. providing nucleation sites or changes in physico-chemical conditions in their respective microenvironments).

Summary and conclusions

Despite our efforts it was not possible to conclusively identify individual secondary As minerals in the Rabbit Lake TMF. Considering the concentration of As in the tailings, the nominal concentration of a possible As-bearing mineral should be $<5\%$, thus preventing identification by XRD. Indirect evidence from sequential extraction analyses suggests the presence of an amorphous Ca-As phase and a possible, but unlikely, minor amount of an amorphous Fe–As phase. The solubility of an amorphous phase is generally much greater than that of its crystalline counterpart and, therefore, geochemical models have to carefully establish the As-phase before choosing thermodynamic data to evaluate solubilities. The use of inappropriate thermodynamic data can have a profound effect on the projected long-term stability of As in mine tailings.

The close association between HFO and As could be clearly demonstrated. HFO was identified to be 2-line ferrihydrite and its XRD pattern geometry indicates a substantial amount of adsorbed As. This is in good agreement with SEM, TEM and sequential extraction analyses that all showed the close association of HFO and As. The adsorption of As onto HFO may be a "blessing in disguise", providing a long-term sink for As. The As stabilizes the HFO with respect to transformations to other oxides (Waychunas and others 1996) and if conditions remain oxidizing, As is not released (Pichler and others 1999).

Up to 20% As in the tailings are present in primary minerals that reach the tailings via the CCD fraction. These are As minerals that were present in the uranium ore and survived the extraction process. The As in these minerals should not be soluble under environmental conditions, present in the tailings (pH $\sim$ 10 and T $\sim$ 0 °C; Donahue and others 1999) and thus, does not pose an environmental hazard.

All secondary As phases are supplied to the tailings via the SOLPA fraction. This is, As that was present in the uranium ore and was dissolved during the extraction process. SOLPA and CCD combined constitute the final tailings material, which is represented by our sample COM. The mixing of SOLPA and CCD may produce slightly different physico-chemical conditions and, therefore could cause either precipitation or dissolution of new As phases. While theoretically possible, this was not observed to be the case in the TMF. The mineralogy and sequential extraction characteristics of COM are more or less identical to those of samples that have already been deposited for several years (477, 481, 539 and 541).

Acknowledgements Thanks to the CAMECO corporation and in particular Pat Landine for the support of this study. Judy Vaive and Pierre Pelchat, Geological Survey of Canada, are thanked for help with the sequential extraction analyses. Ron Hartree at the University of Ottawa provided technical and moral support through the, at times, frustrating XRD experiments and Robert Donahue provided the TMF samples.

References

Arnet JD, Milde G, Kerndorff H, Schleyer R (1989) Waste deposit influences on groundwater quality as a tool for waste type and site selection for final storage quality. In Baccini P (ed) The landfill reactor and final storage, vol 20. Lecture notes in earth sciences, Springer, Berlin Heidelberg New York, pp 399–415

Belzile N, Tessier A (1990) Interactions between arsenic and iron oxyhydroxides in lacustrine sediments. Geochim Cosmochim Acta 54:103–109

Bowell RJ (1994) Sorption of arsenic by iron oxides and oxyhydroxides in soils. Appl Geochem 9:279–286

Boyle RW, Jonasson IR (1973) The geochemistry of arsenic and its use as an indicator element in geochemical prospecting. J Geochem Explor 2:251–296

Chao TT, Theobald JPK (1976) The significance of secondary iron and manganese oxides in geochemical exploration. Econ Geol 71:1560–1569

Chukhrov FV, Groshkov AI, Zirijagin BB, Yermilova LP, Balashova V (1973) Ferrihydrite. Int Geol Rev 16:1131–1143

Deer WA, Howie RA, Zussmann J (1992) An introduction to the rock-forming minerals. Longman Scientific & Technical, Essex

Donahue R, Hendry MJ, Landine P (2000a) Distribution of arsenic and nickel in uranium mill tailings, Rabbit Lake, Saskatchewan, Canada. Appl Geochem 15(8):1097–1119

Donahue R, Hendry MJ, Landine P (2000b) Geochemistry of arsenic and nickel in uranium mill tailings, Saskatchewan, Canada. Appl Geochem (in press)

Drever JI (1988) The geochemistry of natural waters. Prentice-Hall, Englewood Cliffs

Fortin D, Leppard GG, Tessier A (1993) Characteristics of lacustrine diagenetic iron oxyhydroxides. Geochim Cosmochim Acta 57:4391–4404

Foster AL, Brown GE Jr., Tingle TN, Parks GA (1998) Quantitative arsenic speciation in mine tailings using X-ray absorption spectroscopy. Am Mineral 83:553–568

Fuller CC, Davis JA, Waychunas GA (1993) Surface chemistry of ferrihydrite. Part 2. Kinetics of arsenate adsorption and coprecipitation. Geochim Cosmochim Acta 57:2271–2282

Hall GEM, Waive JE, Beer R, Hoashi M (1996) Phase selective leaches for use in exploration, In: Bonham-Carter GF, Galley AG, Hall GEM (eds) A multidisciplinary approach to massive sulphide research in the Rusty Lake-Snow Lake Greenstone Belts, Manitoba, vol 426. Geol Surv Can, Bull, pp 169–200

Jambor JL, Dutrizac JE (1998) Occurrence and constitution of natural and synthetic ferrihydrite, a widespread iron oxyhydroxide. Chem Rev 98:2549–2585

Kelleher E (1994) The stability and solubility of the calcium arsenates in water as a functions of pH at 25 °C. MSc Thesis, University of Waterloo, London

Korte NE, Fernando Q (1991) A review of arsenic (III) in groundwater. Crit Rev Environ Controls 21:1–36

Laguitton, D (1976) Arsenic removal from gold mine waste waters. basic chemistry of the lime addition method. Can Inst Mining Metall Petrol Bull:105–109

Langmuir D, Mahoney J, MacDonald A, Rowson J (1999) Predicting the arsenic source term from buried uranium mill tailings, Tailings and Mine Waste 99. Fort Collins, Colorado

Manning BA, Goldberg S (1997) Adsorption and stability of arsenic(III) at the clay mineral–water interface. Environ Sci Technol 31:2005–2011

Mok WM, Wai CM (1994) Mobilization of arsenic in contaminated river waters. In Nriagu JO (ed) Arsenic in the environment, Part 1, cycling and characterization. Wiley, New York, pp 99–118

O'Neill P (1990) Arsenic. In Pacey GE, Ford JA (eds) Heavy metals in soils. Blackie, Glasgow, pp 83–99

Parker RJ, Nicholson K (1990) Arsenic in geothermal sinters. determination and implications for mineral exploration. In: Harvey CC, Browne PRL, Freestone DH, Scott GL (eds) 12th NZ Geothermal Workshop, Auckland University, Auckland, pp 35–39

Pichler T, Veizer J, Hall GEM (1999) Natural input of arsenic into a coral-reef ecosystem by hydrothermal fluids and its removal by Fe(III) oxyhydroxides. Environ Sci Technol 33:1373–1378

Robins RG (1985) The aqueous chemistry of arsenic in relation to hydrometallurgical processes. Proceedings 15th CIM Annual Meeting, vol 1. Canadian Institute of Mining, Vancouver, pp 1–25

Rosehart R, Lee J (1972) Effective methods of arsenic removal from gold mine wastes. Can Mining J 6:53–57

Scheidegger AM, Strawn DG, Lamble GM, Sparks DL (1998) The kinetics on mixed Ni–Al hydroxide formation on clay and aluminum oxide minerals. a time-resolved XAFS study. Geochim Cosmochim Acta 62:2233–2245

Stumm W, Morgan JJ (1996) Aquatic chemistry. Wiley-Interscience, New York

Taylor RM (1974) The rapid formation of crystalline double hydroxy salts and other compounds by controlled hydrolysis. Clay Mineral 19:591–603

Waychunas GA, Fuller CC, Rea BA, Davis JA (1996) Wide angle X-ray scattering (WAXS) study of "two line" ferrihydrite structure. Effect of arsenate sorption and counterion variation and comparison with EXAFS results. Geochim Cosmochim Acta 60:1765–1781

Webster, JG, Webster, KS (1994) Arsenic adsorption from geothermal bore water, theory and practice. In: Harvey CC, Browne PRL, Freestone DH, Scott GL (eds) 16th NZ Geothermal Workshop, Auckland University, Auckland, pp 65–69